A molecular proximity sensor based on an engineered, dual-component guide RNA

Junhong Choi[1,#], Wei Chen[1,2], Hanna Liao[1,3], Xiaoyi Li[1], Jay Shendure[1,4,5,6,#]

[1] Department of Genome Sciences, University of Washington, Seattle, WA 98195, USA
[2] Institute for Protein Design, University of Washington, Seattle, WA 98195, USA
[3] Molecular and Cellular Biology Program, University of Washington, Seattle, WA 98195, USA
[4] Howard Hughes Medical Institute, Seattle, WA 98195, USA
[5] Brotman Baty Institute for Precision Medicine, Seattle, WA 98195, USA
[6] Allen Discovery Center for Cell Lineage Tracing, Seattle, WA 98195, USA
[#] To whom correspondence should be addressed. Email: junhongc@uw.edu, shendure@uw.edu

Abstract

One of the goals of synthetic biology is to enable the design of arbitrary molecular circuits with programmable inputs and outputs. Such circuits bridge the properties of electronic and natural circuits, processing information in a predictable manner within living cells. Genome editing is a potentially powerful component of synthetic molecular circuits, whether for modulating the expression of a target gene or for stably recording information to genomic DNA. However, programming molecular events such as protein-protein interactions or induced proximity as triggers for genome editing remains challenging. Here we demonstrate a strategy termed P3 editing, which links protein-protein proximity to the formation of a functional CRISPR-Cas9 dual-component guide RNA. By engineering the crRNA:tracrRNA interaction, we demonstrate that various known protein-protein interactions, as well as the chemically-induced dimerization of protein domains, can be used to activate prime editing or base editing in human cells. Additionally, we explore how P3 editing can incorporate outputs from ADAR-based RNA sensors, potentially allowing specific RNAs to induce specific genome edits within a larger circuit. Our strategy enhances the controllability of CRISPR-based genome editing, facilitating its use in synthetic molecular circuits deployed in living cells.

Introduction

Interactions among genes, proteins, and other biomolecules form molecular circuits that process information. Endogenous molecular circuits are composed of different functional modules that can sense, transmit, or integrate various events experienced by cells as inputs. The processed information is used to direct cellular processes, often by altering the expression of specific genes or by inducing chemical modifications to existing molecules (e.g., phosphorylation cascades). One of the goals of the field of synthetic biology is to augment the endogenous molecular circuitry with synthetic components that process specific input signal(s) to desired output(s) in a predictable fashion[1]. For example, various synthetic circuits have been built to modulate gene expression or post-translational modifications, in response to a wide range of input signals such as the presence of specific small molecules[2].

Genome editing is a potentially attractive output for synthetic molecular circuits. Changes in the genome (or epigenome) can alter the expression of specific genes, unlock the synthesis of specific proteins, or simply serve as a record of past events stably etched into genomic DNA[3]. In nature, targeted alterations of genomic DNA are used to record exposure to specific pathogens (e.g., CRISPR) or to generate diversity in recognition

molecules that discriminate self from non-self (e.g., antibodies). In particular, the CRISPR system for immune response in bacteria has been repurposed as a programmable genome editing method[4–6]. Since its initial use for genome editing via a programmable nuclease, various genome and epigenome editing methods have been developed that leverage the CRISPR-Cas9 protein as an integral component. Modifications of the Cas9 protein have facilitated more precise genome editing (e.g., base editing, prime editing) or epigenetic control of gene expression (e.g., CRISPRa, CRIPSRi)[7,8].

A critical feature of CRISPR-based genome editing is its straightforward programmability, as the CRISPR guide RNA (gRNA) molecule alone can specifically program the genomic location to be edited. Prime editing[9] extends this advantage via a prime editing guide RNA (pegRNA) that programs both the target locus and editing outcome. However, to fully realize CRISPR's potential in synthetic molecular circuits, we also require machinery that transduces molecular events into genome editing events. For example, the ENGRAM method transduces the output of transcriptional reporters into signal-specific prime editing events[10]. However, it remains unclear how to develop sensors that trigger specific genome editing outcomes for a broader range of event classes (e.g., protein-protein interactions, exposure to small molecules, gene expression, etc.).

RNA engineering is a promising way to construct molecular sensors. RNA aptamers have been developed to sense exposure to small molecules, both outside and inside living cells[11]. Similar approaches have been taken to engineer the CRISPR-gRNA to sense small molecules[12–14] or the presence of specific RNA molecules via RNA-RNA base-pair interactions[15,16]. The main advantage of engineering the CRISPR-gRNA instead of protein components is the possibility of multiplexing, i.e. linking each molecular sensor to a different genome editing target site and/or editing outcome. However, both the aptamer-based and RNA-sensing sgRNA strategies are limited by the available functionalities of RNA aptamers in the cellular context. In particular, RNA aptamers or RNA-sensing sgRNAs cannot sense the specific proteins or protein-protein interactions that are at the heart of the molecular circuits underlying most cellular processes.

One of the major functionalities of protein molecules is their ability to recognize and interact with their on-pathway binding partners. The function of a protein might be to simply recognize another peptide with high affinity and specificity as in the case of epitope-antibody interaction, or their interactions can be dynamically controlled by post-transcriptional modifications or the presence of small molecules that act as "molecular glues"[17]. Using such protein-sensing elements, one can imagine constructing synthetic circuits that sense protein-based signals to conditionally trigger genome editing of a specific genomic location, possibly in the form of a signal-specific editing outcome. The edit could be used to change the function of a specific gene via insertion/deletion/substitution, to modulate its expression via CRISPRa/i, or to record a memory of the signal into the genome via a "DNA Tape"[18].

Here we present a strategy named "P3 editing" (protein-protein proximity), in which specific protein-protein interactions or proximity events promote the formation of the active CRISPR-gRNA complex. P3 editing is based on the dual-component guide RNA of the native CRISPR-Cas9 system[4], but with the crRNA:tracrRNA dimerization domain replaced with two protein-binding RNA aptamers such as MS2 and BoxB hairpins. Interactions or proximity between two different proteins tagged with MCP (binding MS2 RNA aptamer) and LambdaN (binding BoxB RNA aptamer) domains promote the formation of functional guide RNA to induce genome editing. We demonstrate that P3 editing can be used in concert with both base editing and prime editing, converting known protein-protein interactions into genome-editing events in human cells. Finally, we explore whether P3 editing can be coupled to ADAR-based RNA sensors to control genome editing based on RNA expression, potentially expanding the range of inputs that can be used to drive signal-specific editing in synthetic molecular circuits.

Results

Testing three strategies for leveraging the guide RNA as a dimerization module

To achieve a molecular proximity sensor that drives genome editing, a specific physical interaction between two molecules needs to be converted into a successful genome editing event. One possibility is to "split" a key molecule into two parts, but in such a way that bringing complementary non-functional parts into proximity restores its molecular function. This strategy has been successful in various protein designs[19], such as split-GFP[20], split-Luciferase[21], or split-Protease[22] to convert protein-protein interactions or proximities into various output signals based on fluorescence, bioluminescence, or protein modification. In the split architecture, the "dimerization module" is a key sensor component. In considering how this strategy might be adapted to genome editing, we decided to test whether a guide RNA rather than protein could serve as the dimerization module, i.e. by splitting it into two parts, and making the restoration of its function dependent on a molecular proximity event. In our initial experiments, we focused on the pegRNA used in prime editing.

We considered three broad strategies in designing a "split-pegRNA" system. First, the pegRNA could be split into a functional sgRNA and its 3' extension sequence containing the reverse-transcription template (RTT) and primer binding sequence (PBS), the latter also referred to as prime editing trans RNA or petRNA by a recent report[23] (**Figure 1a**, top). Second, an extra sequence motif such as a self-splicing split-ribozyme could be inserted within the pegRNA sequence, such that the coming together of split-ribozyme parts would be required to splice out the extraneous sequence and yield a functional pegRNA (**Figure 1a**, middle). Third, the pegRNA could be divided at the repeat:anti-repeat junction, which was originally joined with a GAAA RNA tetraloop to form a single-guide RNA (sgRNA) molecule from crRNA and tracrRNA[4] (**Figure 1a**, bottom).

We first tested splitting the pegRNA into a functional sgRNA and petRNA (**Figure 1a**, top; **Supplementary Figure 1a-b**). We reasoned that the addition of complementary RNA sequences as a "dimerization module" at the split junction of sgRNA and petRNA would drive the formation of an active pegRNA complex only when the correct complementary sequences are present. To inhibit early degradation of split RNAs, we appended an additional RNA pseudoknot structure at the ends of both molecules, borrowing from the strategy used to form the enhanced pegRNA or "epegRNA" for higher prime editing efficiency[24]. We tested a handful of RNA:RNA dimerization sequences that range from 13 to 164 base-pairs, with an expectation that base-pairing between dimerization sequences would drive the formation of active pegRNA molecules To measure the editing efficiency of the sgRNA:petRNA splitting strategy, we cloned each RNA in separate RNA-expression vectors. We programmed crRNA:petracrRNA to target the endogenous *HEK3* locus and insert CTT at the +0 position relative to the nick in combination with the "PE4max" prime editor (also referred to as PEmax-P2A-hMLH1dn), as this edit has been previously used to benchmark prime editing[9,25]. In general, we observed a low editing efficiency (<2%) by sgRNA-petRNA pairs that are expected to be dimerized by complementary RNA sequences, even with an additional 3' RNA pseudoknot structure that inhibits RNA degradation from 3' end[24] (**Supplementary Figure 1c**). The inefficiency in editing is unlikely to be due to the inserted dimerization domain because a single pegRNA with additional RNA stem-loop structure at the PE-junction exhibited moderate editing efficiency (~10%; pegRNA w/ SL condition in **Supplementary Figure 1c**). The underlying cause might be the inefficient dimerization driven by RNA-RNA duplex formation in the cellular environment without additional protein binding to the RNA duplex, or possible degradation of RNA duplex that lies outside of the Cas9-gRNA complex, unprotected from other factors for binding.

Second, we tested the idea of inserting self-splicing ribozymes within the pegRNA (**Figure 1a**, middle; **Supplementary Figure 2a**). A potential advantage of this strategy is that splicing out of the ribozyme sequence would result in an identical molecule to the standard pegRNA. We tested 6 sites within pegRNA to insert the whole self-splicing ribozyme sequence from *Tetrahymena thermophila*[26] (413-bp in length)

(**Supplementary Figure 2b**). If this proved successful, we envisioned that the ribozyme could be split into two parts and function as a "split-ribozyme"[27]. However, editing using pegRNAs containing the self-splicing ribozyme sequence was inefficient (<2%) in all 6 constructs. To the limited extent that editing was observed, we found that it was dependent on ribozyme function because including a loss-of-function substitution in the ribozyme sequence reduced editing efficiency by greater than 10-fold (**Supplementary Figure 2c**). Our results suggest that while prime editing depends on the self-splicing function of the ribozyme to produce an active pegRNA, the overall ribozyme efficiency is too low, possibly due to the presence of a prime editing enzyme that might bind and interfere with self-splicing.

Finally, we tried splitting the pegRNA into a crRNA component and a tracrRNA component with the 3'-extension necessary for prime editing (we term the latter as the prime editing tracrRNA or "petracrRNA") (**Figure 1a**, bottom; **Figure 1b**). Previous reports have shown that the distal double-stranded RNA region of the crRNA:tracrRNA junction (also known as the repeat:anti-repeat junction) is not necessary for Cas9 function; this region is replaced by the GAAA tetraloop sequence in the standard sgRNA constructs[4]. Therefore, we replaced this sequence with other complementary RNA sequences and appended an additional RNA pseudoknot structure at the end of both molecules to inhibit early degradation of split RNAs, similar to our testing of sgRNA/petRNA above.

We cloned six pairs of crRNA-petracrRNA pairs, varying sequences that are likely to drive dimerization between crRNA and petracrRNA, but less likely to be essential for interaction between the pegRNA and prime editor (**Figure 1c**). Using the 10-bp dimerization sequence found in the standard sgRNA, we observe editing efficiency at *HEK3* of 15% (**Figure 1d**), which was 37% of the editing efficiency of the standard epegRNA programming of the same edit ("eCTT control") with the same PE4max prime editor. When different dimerization sequences were placed on crRNA and petracrRNA, the editing efficiency varied between 15-25%. The editing efficiency was further enhanced to 28% by flipping A-U pairs at the bottom of repeat:anti-repeat duplex, which is 76% of the editing efficiency of the eCTT control. In contrast, removing the dimerization sequence reduced the editing efficiency to 2.7%, which further reduced to 0.3% when the upper part of the Cas9-binding duplex was removed (**Figure 1c,d**; short-1 and short-2 designs). To verify that the observed editing was dependent on RNA-RNA hybridization, if we paired crRNA and petracrRNA with unmatching dimerization sequences, we consistently observed low editing efficiency (2-3%) (**Figure 1e**).

In summary, we tested three strategies to split the pegRNA into two molecules (**Fig. 1a**). Among these, splitting the pegRNA at the repeat:anti-repeat portion is the most promising strategy, and can be potentially extended to the general gRNA used with CRISPR-Cas9 (**Figure 1a**, bottom; **Fig. 1b-e**). The resulting rates of prime editing are strongly dependent on the complementarity between the repeat:anti-repeat region of crRNA and petracrRNA. Furthermore, our design mimics the functional molecules within the native CRISPR-Cas9 system, initially discovered as the dual-RNA-guided system[4]. Therefore, we pursued this strategy in further developing a molecular proximity sensor that drives genome editing.

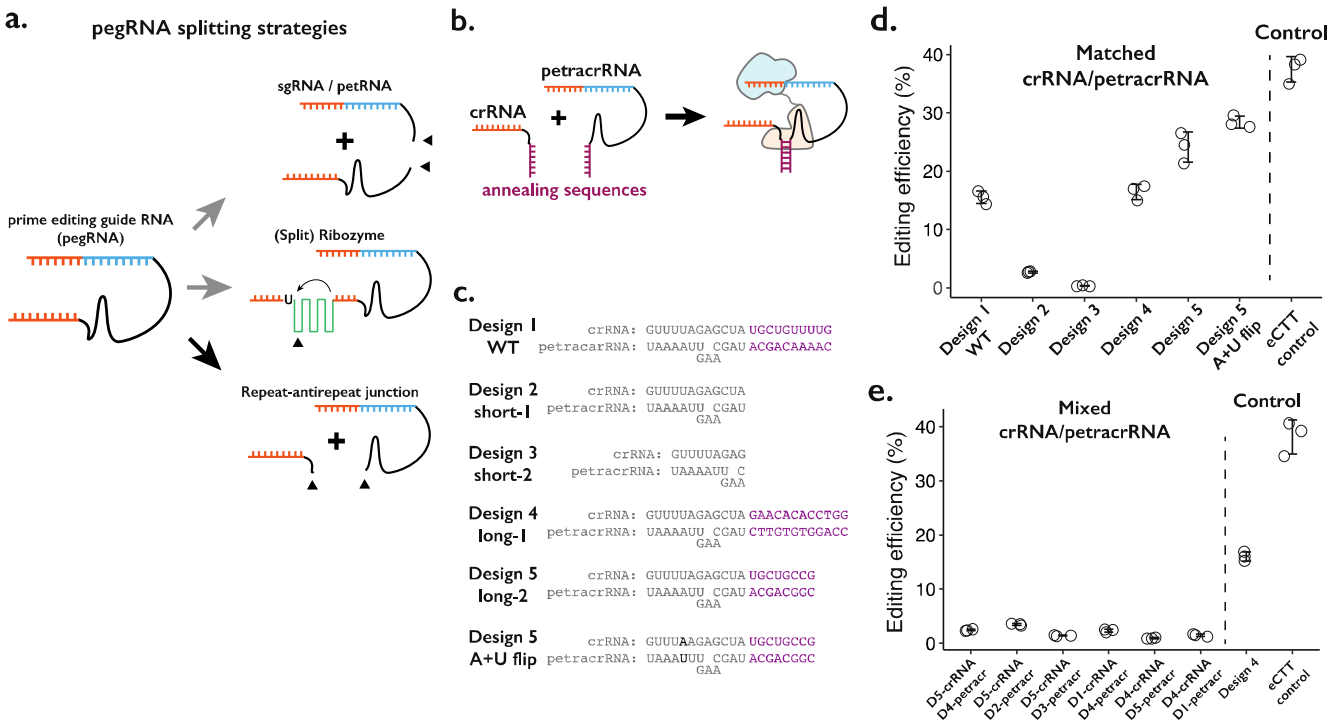

Figure 1. Testing the consequences of splitting the pegRNA at the repeat:anti-repeat junction.

a. We tested three classes of split-pegRNA designs: (top) pegRNA is split to sgRNA and petRNA. (center) Self-splicing ribozyme is inserted into pegRNA, thus splitting it into two parts. (bottom) The Cas9-binding scaffold is split at the crRNA:tracrRNA junction, which is joined through a GAAA RNA tetraloop in the standard sgRNA. **b.** Dimerization of crRNA and prime editing tracrRNA (petracrRNA) for Cas9 activity is guided by RNA annealing sequences (shown in purple) that are complementary. **c.** Different designs of complementary sequences for the crRNA-petracrRNA interaction. **d-e.** Editing efficiencies for prime editing (CTT insertion to HEK3 native genomic locus) using matching (**d**) or mixed (**e**) crRNA/petracrRNA pairs. CTT insertion efficiency using epegRNA was used as the positive control ("eCTT control").

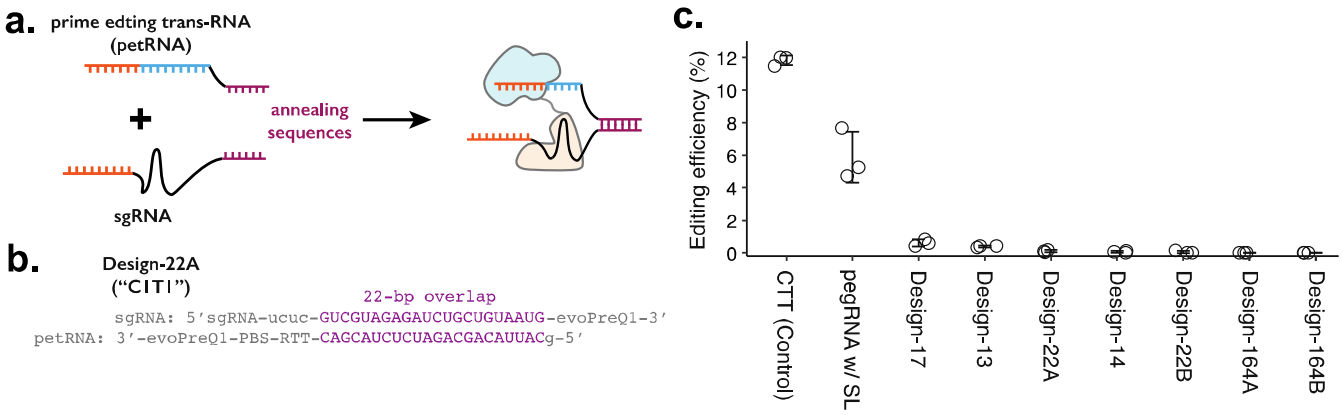

Supplementary Figure 1. Testing the sgRNA:petRNA splitting strategy.

a. Schematic of splitting functional pegRNA into sgRNA with extended sequence on 3'-end and petRNA with extended sequence on 5'-end for controlling dimerization. Annealing of two dimerization sequences would result in an active pegRNA. **b.** Example design of dimerization sequence. Each design is named after the length of the reverse-complementary sequence (22-bp shown here). In both sgRNA and petRNA, evoPreQ1 RNA pseudoknot domains are added to reduce the degradation of the non-Cas9-bound RNA portion. **c.** The editing efficiency was measured for seven different sgRNA:petRNA pairs along with prime editing control (pegRNA targeting HEK3 locus for CTT insertion at +0 position from the nick) and a single pegRNA construct with 22-bp RNA stem-loop between the sgRNA and RTT portion (pegRNA w/ SL) to test whether having extra RNA-duplex affects the prime editing efficiency.

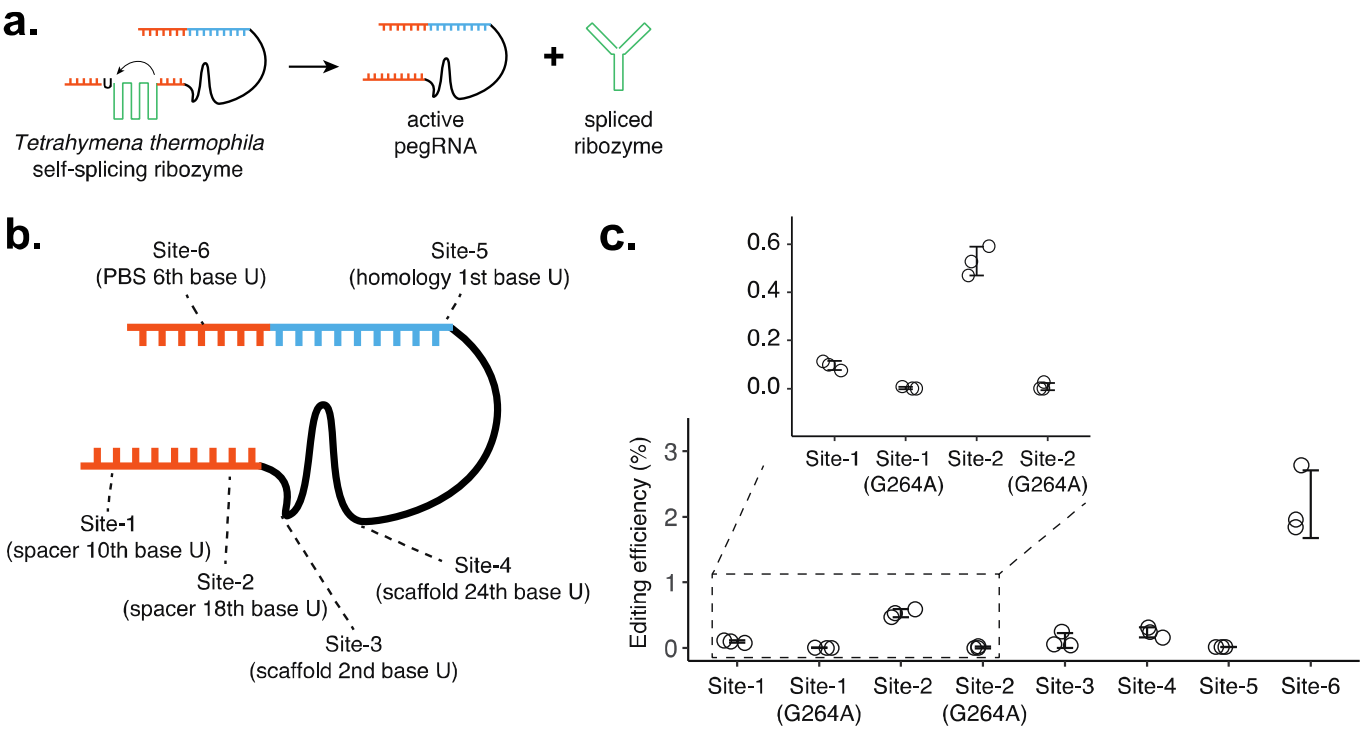

Supplementary Figure 2. Testing the self-splicing ribozyme strategy.

a. Schematic of self-splicing ribozyme strategy. Insertion of the ribozyme into functional pegRNA would lead to self-splicing after RNA transcription, which would result in an active pegRNA and spliced ribozyme sequence. If this worked, the ribozyme could be further split into two functional parts, where extra dimerization domains can be added to control ribozyme function. **b.** Six positions within the pegRNA (targeting HEK3 locus for CTT insertion) were tested for inserting the self-splicing ribozyme sequence. Ribozyme needs to start with a uridine base for splicing, which remains after the ribozyme is spliced out. **c.** Editing efficiencies were measured for 6 ribozyme insertion sites within pegRNA. For Site-1 and Site-2, two additional designs were constructed with inactive ribozyme (G264A mutation).

Controlling genome editing with protein-protein proximity

To convert protein-protein interaction events into genome editing events, we reasoned that the RNA dimerization domain within crRNA and tracrRNA could be replaced with an RNA-based protein dimerization domain, such that specific protein-protein interactions or prolonged proximity would aid in the formation of active gRNA that would then bind to Cas9 (**Figure 2a**). To date, many specific protein-RNA interaction parts have been identified, including the MS2 RNA aptamer that binds to the MCP domain[28]. Among different RNA-protein pairs, we chose two pairs, MS2-MCP and BoxB-LambdaN[29–31], which can be used as adaptors for using protein-protein interactions to drive RNA-RNA interactions.

We designed a crRNA and petracrRNA pair, for which previously identified dimerization sequences of the upper portion of the repeat:anti-repeat duplex were replaced with MS2 and BoxB RNA aptamers. To aid the formation of the proper bulge within the RNA duplex (A and AAG in crRNA and petracrRNA, respectively), we replaced the original sequence of GCUA in crRNA with GCGC, and UAGC in petracrRNA with GCGC. Finally, we added evoPreQ1 RNA pseudoknot sequence on both RNA molecules to reduce RNA degradation from 3'-ends, resulting in crRNA-MS2 and BoxB-petracrRNA.

To test whether crRNA and petracrRNA modified with protein-binding aptamer sequences can be used to drive genome editing, we constructed a single protein where the MCP and LambdaN domains were fused with a flexible linker (MCP-LambdaN), with the intent of bringing crRNA-MS2 and BoxB-petracrRNA into close proximity to form active pegRNA. When we transfected HEK293T cells with plasmids expressing MCP-LambdaN, PE4max[25], crRNA-MS2, and BoxB-petracrRNA that targets *HEK3* locus and programs for CTT insertion at +0 position, we observed 15% editing efficiency, which was 52% of the editing rate achieved by transfecting a single, standard epegRNA-expressing plasmid that programs the same edit along with the PE4max-expressing plasmid ("eCTT control") (**Figure 2b**). When the MCP-LambdaN-expression plasmid was substituted with a GFP-expressing filler plasmid ("Filler GFP plasmid" condition in **Fig. 2b**), editing efficiency dropped to 6% of the eCTT control, indicating that crRNA-MS2 and BoxB-petracrRNA can promote genome editing to a limited extent, presumably by forming an active pegRNA complex even without the additional dimerization domain.

We next sought to extend this approach to link arbitrary protein-protein interactions to genome editing. For this, we designed protein components that can induce the formation of pegRNA complexes containing crRNA-MS2 and BoxB-petracrRNA. As above, because the editing efficiency can vary depending on the transfection efficiency (30-60% depending on the culturing condition and confluency of the cell culture), we continued to use a "normalized editing efficiency" scale where the observed editing efficiency is scaled to the eCTT control to facilitate comparison across experiments.

We selected three known pairs of interacting protein domains and appended MCP and LambdaN domains with several nuclear localization sequences[25]: 1) GCN4 epitope sequence (20 AA) and single-chain variable fragment[32–35] (scFv; 250 AA) that recognizes GCN4 epitope, 2) ALFA-tag sequence (15 AA) and nanobody specific for ALFA-tag[36] (NbALFA; 135 AA), and 3) split-GFP[20,37], where 11 beta-sheets of GFP is split into GFP1-10 (220 AA) and GFP11 (17 AA). For the GCN4 epitope design, we constructed two designs where either a single repeat of the epitope (1xGCN4) was used, or four repeats of the epitope (4xGCN4) were strung together, as often done to increase the efficiency of scFv binding to the tagged protein molecule. For the split-GFP design, we also constructed a version without any nuclear localization sequences, to test whether protein localization also affects editing efficiency. Designed proteins were cloned into protein expression plasmids and transfected into cells along with crRNA/petracrRNA/prime editor expressing plasmids.

First, we observe that both epitope-antibody/nanobody interactions were able to induce strong genome editing efficiencies, close to the levels observed with the MCP-LambdaN fusion protein (**Figure 2b**).

Interestingly, the additional GCN4 epitopes in the 4xGCN4 design did not seem to increase editing efficiency, possibly meaning either that GCN4:scFv binding is saturated and additional GCN4 epitopes do not make a difference in bringing crRNA and petracrRNA into proximity, or that only the scFv binding to one of GCN4 epitope contributes to the active pegRNA formation due to spatial constraints. Second, we observe that split-GFP designs generally have lower editing efficiency, possibly due to weaker interaction between GFP1-10 and GFP11 compared to epitope-antibody/nanobody interactions. Finally, all three protein pairs as well as MCP-LambdaN fusion constructs include nuclear localization sequences to enhance genome editing in the nucleus. We also tested the split-GFP construct without a nuclear localization sequence, which resulted in an even lower editing efficiency, possibly indicating that the nuclear-localization propensity of proteins tagged with the MCP or LambdaN could affect the effectiveness of P3 editing.

Lastly, we tested whether this strategy could be adapted to facilitate small molecule-based control of genome editing. In the past 30 years, several chemicals have been identified as critical signaling molecules for promoting protein-protein interactions[17]. We reasoned that the addition of such chemicals to cell culture could be used to control genome editing of specific targets and editing outcomes. To demonstrate the chemical control of P3 editing, we chose Rapamycin-induced dimerization of FKBP and FRB protein domains of the mTOR pathway[38–40] from human proteome, and Abscisic acid (ABA)-induced dimerization of pyrabactin resistance domain (PYL) and ABA-insensitive (ABI) domain found in plant[41] (**Figure 2c**). We observed a strong increase in the editing efficiency of the FKBP-FRB and PYL-ABI pairs upon the addition of small molecules that induce dimerization (**Figure 2d**). For example, we observed 3.9-fold higher editing upon the addition of 200 uM rapamycin to the FKBP-FRB pair compared to no rapamycin condition (58% vs. 15% normalized editing efficiency), and 2.7-fold higher editing upon the addition of 100 uM ABA to the PYL-ABI pair compared to no ABA condition (36% vs. 13% normalized editing efficiency) (**Figure 2d**).

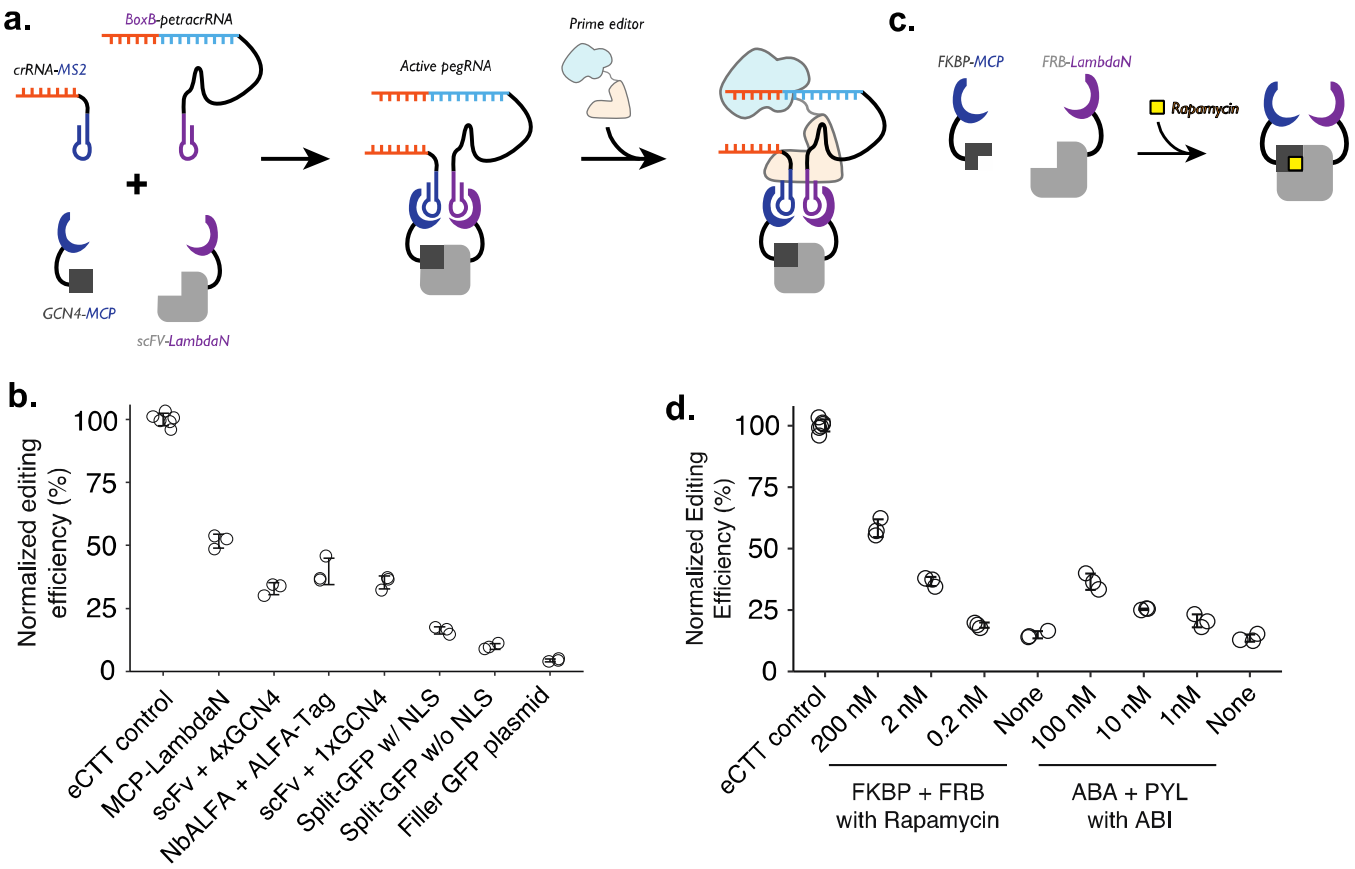

Figure 2. Controlling genome editing with constitutive or chemically-induced protein-protein interactions.

a. Schematic of P3 editing, which couples protein-protein interactions to genome editing. The binding of two proteins (e.g., MCP-tagged GCN4 epitope and LambdaN-tagged scFv) brings two RNA species (e.g., crRNA-MS2 and BoxB-petracrRNA) into close proximity to form an active pegRNA complex, which binds to the prime editor for genome editing. **b.** Normalized editing efficiencies measured with different protein pair interactions. Editing efficiencies were normalized to a consistent eCTT control included in each experiment (left-most). Transfection of filler GFP-expressing plasmid instead of proteins tagged with MCP/LambdaN was used to quantify the background levels of editing as a negative control (right-most). **c.** Using chemically-inducible dimerization to control genome editing. For example, FKBP and FRB domains dimerize in the presence of the small molecule Rapamycin. **d.** Normalized editing efficiencies measured for chemically-induced genome editing.

Optimizing the efficiency vs. specificity trade-off of P3 editing

Overall, these experiments demonstrate that P3 editing can be used to control genome editing via specific interactions between a pair of tagged protein domains. Next, we sought to improve the efficiency and specificity of P3 editing by engineering the crRNA-MS2/BoxB-petracrRNA design. We designed 12 pairs of crRNA-MS2/BoxB-petracrRNA, varying the base composition and length of the upper 4-bp region within the Cas9-binding region of repeat:anti-repeat duplex. Each RNA design was cloned into an RNA expression vector with flanking U6 promoter and TTTTTTT terminator sequences. We transfected HEK293T cells with the mix of four plasmids expressing each component: crRNA-MS2, BoxB-petracrRNA, PE4max, and either split-GFP (GFP1-10 tagged with MCP and GFP11 tagged with LambdaN; to measure the editing efficiency induced by protein-protein interaction) or standard GFP (to measure the background level of editing without protein-protein interaction).

Across 12 designs, we observe a tradeoff between efficiency (ranging between 2% to 53% of normalized eCTT control) and specificity (background editing level without the addition of tagged protein pair ranging between 0.3% to 35%). The efficiency increases with a higher number of G-C base-pairs and annealing length within the varied region, supporting our hypothesis that crRNA-MS2 and BoxB-petracrRNA can form an active pegRNA complex without the addition of protein-mediated proximity, although at a lower rate. However, as the efficiency of P3 editing decreases, the specificity of P3 editing to protein-protein interaction can increase. For example, in our design that uses GAUA:UAUC pairing, we observe 3.8 ± 1.0% normalized editing efficiency with the addition of tagged split-GFP protein, and only 0.27 ± 0.07% normalized editing efficiency without it, a 14-fold increase driven by specific protein-protein interaction. Our optimization effort suggests that the efficiency and specificity of P3 editing can be tuned using different designs of crRNA-MS2/BoxB-petracrRNA, depending on the experimental goal.

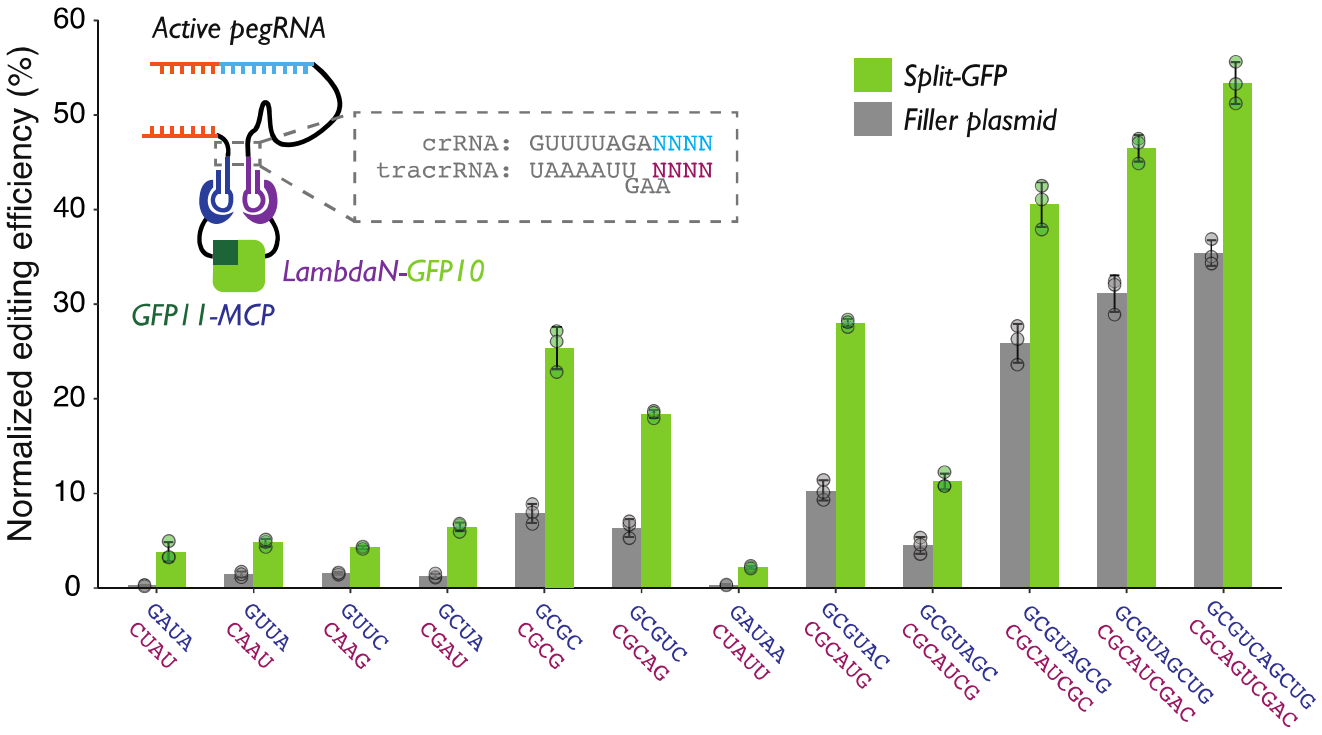

Supplementary Figure 3. Characterizing linkers for crRNA-MS2 and BoxB-petracrRNA.

The upper four base pairs of the Cas9-binding region of repeat:anti-repeat duplex were altered to generate 12 pairs of crRNA-MS2/BoxB-petracrRNA designs. The editing efficiency is normalized with the eCTT positive control included in each experiment (targeting HEK3 locus with CTT insertion at position +0 using standard epegRNA), to control for variable transfection efficiencies. Two normalized editing efficiencies were measured for each pair of RNAs: one with tagged split-GFP to promote dual-RNA-guide formation, and one with standard, untagged GFP to measure the background editing level non-specific to protein-protein proximity.

Coupling various modes of genome editing to protein-protein proximity

While our demonstrations so far coupled the P3 strategy to prime editing, we reasoned that the same strategy could be adapted to other precision editing methods such as base editing (**Figure 3a**). To confirm this, we tested 3 different base editors (CBE2[42], CBE4max[43], and ABE8[44]), which can target the HEK3 locus and make either C-to-T or A-to-G edits (**Figure 3b**). To facilitate compatibility with base editing, we designed BoxB-tracrRNA that lacks the 3'-extension specific to prime editing and cloned it into an RNA expression vector with a U6 promoter. We transfected HEK293T cells with a mix of plasmids expressing: crRNA-MS2, BoxB-tracrRNA, one of the three base editors, and either the LambdaN-MCP fusion protein that brings crRNA-MS2 and BoxB-tracrRNA into close proximity or GFP to serve as a negative control and measure the base-level editing efficiency without a protein component that aids the formation of gRNA complex.

For all three base editors tested, we observe that the addition of LambdaN-MCP increases the editing efficiency (**Figure 3c, left**), although the change in the editing was greater for CBE4max (3.5-fold increase) and ABE8 (2.1-fold increase) than CBE2 (1.4-fold increase). The observed differences are possibly related to different endonuclease activity, as CBE2 uses deactivated Cas9 instead of Cas9 nickase as in the case of the prime editor and other base editors. Of note, the observed genome editing efficiencies of the P3 strategy for all three base editors (**Figure 3c, left**) are comparable to our base editing efficiencies measured with standard single-guide RNA (sgRNA) (**Figure 3c, right**), despite the fact that the P3 strategy uses a 3-component system (using crRNA-MS2, BoxB-petracrRNA, and LambdaN-MCP) instead of one sgRNA.

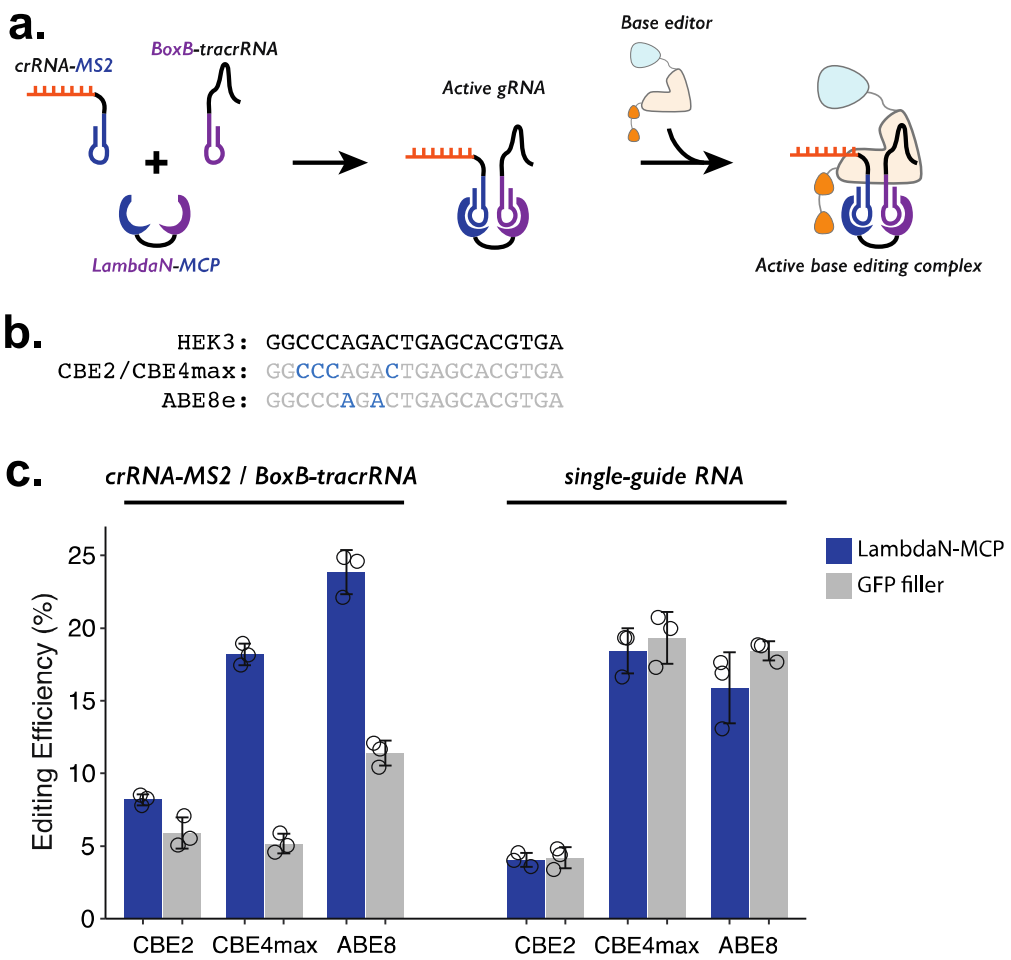

Figure 3. Testing P3 editing strategy in the context of base editing.

a. Schematics of P3 editing strategy adapted to base editing. The LambdaN-MCP fusion protein will bring crRNA-MS2 and BoxB-tracrRNA in close proximity to aid gRNA complex formation, which then binds to the base editor for genome editing. **b.** Cytosine and Adenosine residues targeted by base editing are highlighted within the target HEK3 sequence. **c.** Editing efficiency measured with P3 editing (left) and standard sgRNA (right). For each base editor and guide-RNA combination, editing efficiencies were measured with either LambdaN-MCP expressing plasmid (blue) or a filler plasmid expressing GFP (gray).

Combining ADAR-based editing with P3 editing to control genome editing with RNA expression

In both prime editing and base editing demonstrations of the P3 strategy, we used the presence of LambdaN-MCP fusion protein to control the genome editing efficiency, forming a synthetic circuit with the input of protein expression and the output of genome editing. Recently, a similar synthetic circuit was developed using ADAR-based RNA editing, where the input of specific target RNA expression can be used to control an output of cargo protein expression. In this system (termed CellREADR[45], RADAR[46], or RADARS[47]) an ADAR-guide-RNA is specifically designed to bind the target RNA molecule and promote an RNA base editing event that converts an internal stop codon into a sense codon within the ADAR-guide-RNA, thus initiating cargo protein expression.

To combine the ADAR-based RNA sensor and P3 editing concepts, we programmed the cargo protein downstream of the ADAR-guide-RNA to be a fusion protein (e.g., LambdaN-MCP) that is capable of crRNA and petracrRNA in close proximity (**Figure 4a**). We based our design on the RADARS strategy, which includes an MS2 RNA structure within the ADAR-guide-RNA to aid the recruitment of MCP-tagged ADAR and suppress translation read-through of an internal stop codon. To avoid complications of using MS2 RNA elements in both ADAR-guideRNA and crRNA, we switched out the MS2/MCP pairing with the PP7 RNA element that binds to the PCP protein[48–50] domain, and confirmed that this could support P3 editing (**Figure 4b**). We used an ADAR-guide-RNA design that detects IL6 mRNA expression from the RADARS system[47] because the efficiency and specificity of RNA detection have been previously well-characterized in the context of the cargo protein expression of luciferase and GFP.

In combining RADARS with P3 editing, we transfected HEK293T cells with a mix of six plasmids that express: MCP-ddADAR, ADAR-guide-RNA-LambdaN-PCP (also referred to as ogRNA in RADARS), IL6 RNA for target RNA (specifically chosen in RADARS system because it is not natively expressed in HEK293T cells) crRNA-PP7, BoxB-petracrRNA, and PE4max (**Figure 4c**). We observed the normalized editing efficiency of 11.6 ± 0.7%, which was substantially higher than a condition where the IL-6 RNA-expressing plasmid has been replaced with a filler GFP-expression plasmid (8.2 ± 0.3%) (**Figure 4d**).

While our result suggests that we can control genome editing with specific RNA expression events by combining RADARS and P3 editing, we investigated what contributes to the high background level as well as the low editing efficiency. First, when we replace the plasmid expressing ADAR-guide-RNA-LambdaN-PCP with the ADAR-guide-RNA-GFP (with the cargo protein of GFP instead of LambdaN-PCP), we observe the normalized editing efficiency of 5.5 ± 0.6% (**Figure 4d**). This suggests that the crRNA-PP7 and BoxB-petracrRNA can induce 5.5% normalized editing efficiency without LambdaN-PCP in the system, characterizing the non-specific editing level of P3 editing, and suggesting that the remaining 2.7% of normalized editing efficiency background is due to non-specific editing of the RADARS system, possibly due to leaky expression of LambdaN-PCP even in the absence of IL6 target RNA. Finally, when we replace 50% of ADAR-guide-RNA-GFP expression plasmid with LambdaN-PCP expression plasmid, we observe the normalized editing efficiency to increase up to 34 ± 1%, suggesting that the inclusion of the RNA-controlled protein expression module might be lowering the overall editing efficiency. Overall, these results suggest that while the P3 editing strategy can be combined with other synthetic circuits to control genome editing with various inputs, the efficiency and specificity of control may degrade over combinations of multiple synthetic modules, and that further optimization is necessary.

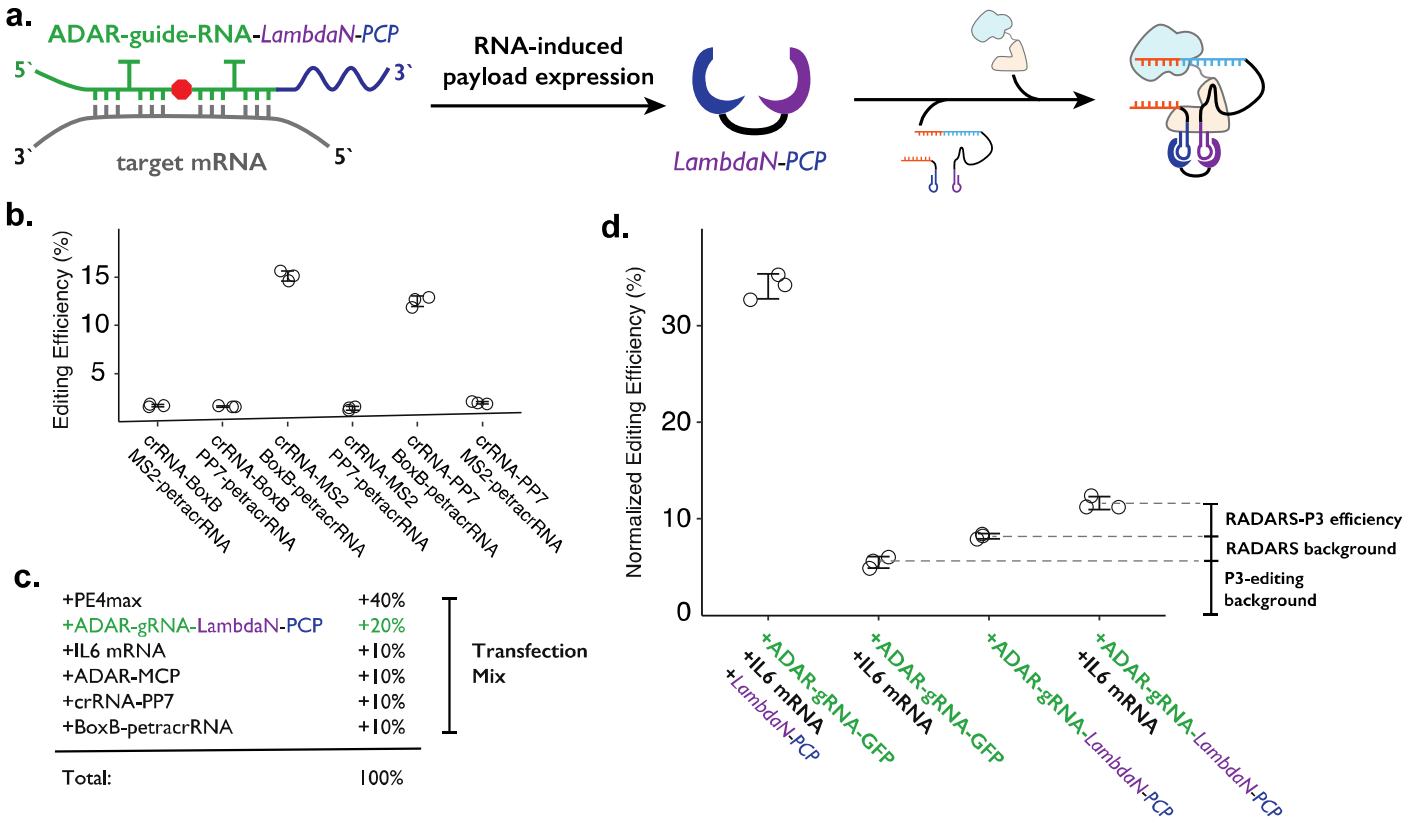

Figure 4. Combining ADAR-based RNA sensors with P3 editing.

a. Schematics of combining ADAR-based RNA sensors with P3 editing. ADAR-guide-RNA senses target RNA by forming extended RNA duplex based on reverse-complementary sequence, which is a substrate for RNA editing by ADAR. RNA editing converts the in-frame stop codon into a sense codon, which then starts the expression of cargo protein. In combination with P3 editing, the cargo protein will be LambdaN-PCP, which will then help prime editing complex formation by bringing crRNA-PP7 and BoxB-petracrRNA together. **b.** The six pairs of crRNA/petracrRNA with three different RNA aptamers (BoxB, MS2, and PP7) were tested for P3 editing, to avoid using MS2 RNA element in P3 editing, as it is used in RADARS strategy for the ADAR-based RNA sensing. **c.** Composition of transfection condition with six expression plasmid. The percentage is based on the mass amount of plasmid added to the transfection mix. **d.** The normalized editing efficiency was measured to characterize the efficiency and specificity of ADAR-based RNA sensing and P3 editing strategy.

Discussion

Molecular sensors expand our ability to capture and observe biological events as they unfold within living cells[2,51,52]. Key parameters to consider in using molecular sensors include their efficiency and specificity in converting events-of-interest into measurable output. Although various sensors of RNA or protein production have been developed, the readout is almost always in the form of luminescence or fluorescence (e.g., luciferase or GFP in the case of RADARS[47]), because microscopy- or flow-sorting-based detection methods are common modes of detection with high sensitivity, possibly overcoming low conversion efficiency by sensors as long as they have high specificity.

For several reasons, genome editing is an attractive alternative for recording the output of molecular sensors[3,10,53,54]. First, massively parallel sequencing is a low-cost means of acquiring data, and any low conversion efficiency could potentially be overcome simply through deeper sequencing. Second, single-cell resolution can be achieved by coupling recovery of genome editing events with methods such as single-cell RNA-seq. This affords the potential to recover measurements from much larger numbers of cells than would be possible with microscopy or flow, and moreover to co-assay other classes of information about each cell. Third, information encoded within the genome is maintained and replicated throughout the life cycle of the cell, allowing storage of past information with minimal information loss. On a related point, strategies such as DNA Typewriter[18] can facilitate the time-resolved recording of the output of multiple sensors to a common location(s) in the genome. Finally, molecular sensors can be used to control cellular function as components of synthetic biological circuits. Outputting molecular sensors to genome editing events may facilitate the design of such control structures, particularly as the range of cellular activities that can be programmed by genome editing is rapidly expanding.

In P3 editing, molecular interactions are sensed and converted directly into a genome editing output. We demonstrated that specific RNA-RNA (e.g., annealing of two sequences within crRNA and petracerRNA), RNA-protein (e.g., MS2:MCP and BoxB:LambdaN interactions), and protein-protein (epitope:antibody or chemically-induced dimerization) interactions can be used to control genome editing. Because the input of P3 editing is at the protein level, one could also chain different sensors with protein outputs upstream[2], although the conversion efficiency and specificity may be compounded and result in higher noise in capturing signals through more relays. Finally, the sensor elements in the P3 editing strategy are focused on engineering each CRISPR-gRNA while leaving the gene editor (i.e., prime editor and base editor) unaltered, potentially facilitating multiplex genome editing within the same cell. For example, one could imagine developing a P3 editing strategy to construct a sensor specific to a cell state and combine it with other molecular signal or lineage recording methods[10,18] to reconstruct the past history of each cell.

In our view, the outstanding challenges for P3 editing relate to the efficiency-vs-specificity tradeoff, and the development of sensors compatible with multiplex P3 editing within the same cell. While we characterized the efficiency and specificity of current P3 editing designs, we envision that they could be improved further. For example, the docking of RNA-aptamers such as MS2, BoxB, or PP7 could likely be improved by testing more linker sequences that place crRNA and petracrRNA at a better placement for duplex formation. Also, the current P3 editing design used a pair of RNA aptamers and their corresponding protein binder. While we have identified two such pairs that are compatible with P3 editing (MS2/BoxB and PP7/BoxB), more orthogonal protein-RNA pairs need to be identified (e.g., using a massively parallel platform[55] and/or computational prediction[56]). This could allow for large numbers of P3 sensors for different protein-protein interactions to be deployed within the same cell.

Endnotes

Acknowledgments

We thank members of the Shendure Lab, as well as members of the Allen Discovery Center for Cell Lineage Tracing, for helpful discussions. This work was supported by a grant from the Paul G. Allen Frontiers Group (Allen Discovery Center for Cell Lineage Tracing to J.S.), the National Human Genome Research Institute (UM1HG011586 and R01HG010632 to J.S. and K99HG012973 to J.C.). H.L. is supported by the NSF Graduate Research Fellowship Program (DGE-2140004). J.C. was a Howard Hughes Medical Institute Fellow of the Damon Runyon Cancer Research Foundation (DRG-2403-20), which supported a part of this manuscript. J.S. is an Investigator at the Howard Hughes Medical Institute.

Author contributions

J.C. conceived the project with inputs from J.S. and W.C. J.C. and J.S. designed experiments. J.C. performed experiments with assistance from W.C., H.L., and X.L. J.C. analyzed the experimental results with inputs from J.S. and W.C. J.C. and J.S. wrote the manuscript with inputs from all other authors.

Competing interests

The University of Washington has filed a patent application based on this work, in which J.C., W.C., and J.S. are listed as inventors. J.S. is a scientific advisory board member, consultant, and/or co-founder of Cajal Neuroscience, Guardant Health, Maze Therapeutics, Camp4 Therapeutics, Phase Genomics, Adaptive Biotechnologies, Scale Biosciences, Sixth Street Capital, Pacific Biosciences, and Prime Medicine. The remaining authors declare no competing interests.

Data availability statement

Raw sequencing data have been uploaded to Sequencing Read Archive (SRA) with the associated BioProject ID PRJNA1004865. The following plasmids have been deposited to Addgene: pU6-crRNA-MS2, pU6-BoxB-petracrRNA, pCMV-LambdaN-MCP, pCMV-LambdaN-NbALFA, and pCMV-ALFA-MCP (Addgene ID 207624 - 207628).

Materials and Methods

Plasmid cloning

All crRNA and petracrRNA constructs were cloned using ligation after restriction (T4 DNA Ligase, New England Biolabs), following the protocol outlined in Anzalone *et al.*[9]. Single-stranded DNAs (IDT) were annealed to have 4 bp overhangs in both ends of double-stranded DNAs, which is a substrate for T4 DNA ligase. The plasmid backbone (pU6-pegRNA-GG-acceptor, Addgene #132777) was digested using BsaI-HFv2, and mixed with annealed double-stranded DNA constructs with 4-bp overhangs. At the end of all crRNA and petracrRNA constructs, we added the evoPreQ1 sequence and poly-T terminator sequence. A small amount (1-2 uL) of T4 ligation reaction mix was added to NEB Stbl cell (C3040) for transformation and grown at 37°C for the plasmid DNA preparation (Qiagen miniprep). The resulting plasmids were sequence-verified using Sanger sequencing (Genewiz). Sequences for cloning CRISPR gRNA are included in the "Supplementary Sequences".

All protein expression constructs were cloned using Gibson assembly (NEB, where double-stranded DNA fragments are either ordered from IDT as gBlocks or PCR amplified from existing constructs with at least 25-bp overlap in sequence. A small amount (1-2 uL) of Gibson Assembly reaction mix was added to NEB Stbl cell (C3040) for transformation and grown at 30°C or 37°C for the plasmid DNA preparation (Qiagen miniprep). The resulting plasmids were sequence-verified using Sanger sequencing (Genewiz).

Tissue culture, transfection, lentiviral transduction, and transgene integration

The HEK293T cell line was purchased from ATCC, and maintained by following the recommended protocol from the vendor. HEK293T cells were cultured in Dulbecco's modified Eagle's medium (DMEM) with high glucose (GIBCO), supplemented with 10% fetal bovine serum (Rocky Mountain Biologicals) and 1% penicillin-streptomycin (GIBCO). Cells were grown with 5% CO2 at 37°C. Cell lines were used as received without authentication or a test for mycoplasma.

For transient transfection, HEK293T cells were cultured to 70-90% confluency in a 24-well plate. For prime editing with crRNA/petracrRNA and without protein components, 375 ng of PE4max enzyme plasmid (Addgene #174828), 62.5 ng of crRNA plasmid, and 62.5 ng of petracrRNA plasmid were mixed, and prepared with a transfection reagent (Lipofectamine 3000) following the recommended protocol from the vendor. For transfection with protein components, 250 ng of PE4max enzyme plasmid, 125 ng of protein (MCP-LambdaN, GFP filler plasmid, or 62.5 ng each of two MCP/LambdaN-tagged protein domains), 62.5 ng of crRNA plasmid, and 62.5 ng of petracrRNA plasmid were used in transfection. The transfection mix composition for the experiment with the ADAR-based RNA sensor is described in Figure 4c. Cells were cultured for three to four days after the initial transfection, and their genomic DNA was harvested following cell lysis and protease protocol from Anzalone et al.[9].

Genomic DNA collection and sequencing library preparation

The targeted region from collected genomic DNA was amplified using two-step PCR and sequenced using the Illumina sequencing platform (NextSeq). The first PCR reaction (KAPA Robust polymerase) included 1.5 uL of cell lysate, and 0.04 to 0.4 uM of forward and reverse primers in a final reaction volume of 25 uL. We programmed the first PCR reaction to be: (1) 3 minutes at 95 °C, (2) 15 seconds at 95 °C, (3) 10 seconds at 65 °C, (4) 90 seconds at 72 °C, (5) 25-28 cycles of repeating step 2 through 4, and (6) 1 minute at 72°C. Primers

included sequencing adapters to their 3´-ends, appending them to both termini of PCR products that amplified genomic DNA. After the first PCR step, products were added to the second PCR reaction that appended dual sample indexes and flow cell adapters. The second PCR reaction program was identical to the first PCR program except we ran it for only 5-10 cycles. Products were purified using AMPure and assessed on the TapeStation (Agilent) before being denatured for the sequencing run.

Genomic DNA amplicon sequencing data processing and analysis

Sequencing reads from Illumina NextSeq platform are first demultiplexed using BCL2fastq software (Illumina). Sequencing libraries were single-end sequenced to cover the DNA Tape from one direction. Editing efficiencies were calculated using pattern-matching software such as Regular Expression (package *REGEX*) in Python, counting correct amplicon reads with or without intended edits. For prime editing, CTT insertions to the HEK3 locus[9] were counted, and editing efficiencies were calculated by: reads with CTT insertions / all reads matching the HEK3 locus. In quantifying base editing efficiencies, we first used CRISPResso to identify the top 10 base editing outcome of the HEK3 locus, and used these editing patterns to calculate editing efficiency as follows: all reads matching the top 10 base editing outcomes / all reads matching HEK3 locus.

References

1. Wang, Y.-H., Wei, K. Y. & Smolke, C. D. Synthetic biology: advancing the design of diverse genetic systems. *Annu. Rev. Chem. Biomol. Eng.* **4**, 69–102 (2013).
2. Chen, Z. & Elowitz, M. B. Programmable protein circuit design. *Cell* **184**, 2284–2301 (2021).
3. Sheth, R. U. & Wang, H. H. DNA-based memory devices for recording cellular events. *Nat. Rev. Genet.* **19**, 718–732 (2018).
4. Jinek, M. *et al.* A Programmable Dual-RNA–Guided DNA Endonuclease in Adaptive Bacterial Immunity. *Science* **337**, 816–821 (2012).
5. Cong, L. *et al.* Multiplex genome engineering using CRISPR/Cas systems. *Science* **339**, 819–823 (2013).
6. Mali, P. *et al.* RNA-guided human genome engineering via Cas9. *Science* **339**, 823–826 (2013).
7. Gilbert, L. A. *et al.* CRISPR-mediated modular RNA-guided regulation of transcription in eukaryotes. *Cell* **154**, 442–451 (2013).
8. Gilbert, L. A. *et al.* Genome-Scale CRISPR-Mediated Control of Gene Repression and Activation. *Cell* **159**, 647–661 (2014).
9. Anzalone, A. V. *et al.* Search-and-replace genome editing without double-strand breaks or donor DNA. *Nature* **576**, 149–157 (2019).
10. Chen, W. *et al.* Multiplex genomic recording of enhancer and signal transduction activity in mammalian cells. *bioRxiv* 2021.11.05.467434 (2021) doi:10.1101/2021.11.05.467434.
11. Dykstra, P. B., Kaplan, M. & Smolke, C. D. Engineering synthetic RNA devices for cell control. *Nat. Rev. Genet.* **23**, 215–228 (2022).
12. Tang, W., Hu, J. H. & Liu, D. R. Aptazyme-embedded guide RNAs enable ligand-responsive genome editing and transcriptional activation. *Nat. Commun.* **8**, 15939 (2017).
13. Kundert, K. *et al.* Controlling CRISPR-Cas9 with ligand-activated and ligand-deactivated sgRNAs. *Nat. Commun.* **10**, 2127 (2019).
14. Iwasaki, R. S., Ozdilek, B. A., Garst, A. D., Choudhury, A. & Batey, R. T. Small molecule regulated sgRNAs enable control of genome editing in E. coli by Cas9. *Nat. Commun.* **11**, 1394 (2020).
15. Pelea, O., Fulga, T. A. & Sauka-Spengler, T. RNA-Responsive gRNAs for Controlling CRISPR Activity:

Current Advances, Future Directions, and Potential Applications. *CRISPR J* **5**, 642–659 (2022).

16. Wang, W.-J. *et al.* Establishing artificial gene connections through RNA displacement-assembly-controlled CRISPR/Cas9 function. *Nucleic Acids Res.* (2023) doi:10.1093/nar/gkad558.
17. Schreiber, S. L. The Rise of Molecular Glues. *Cell* **184**, 3–9 (2021).
18. Choi, J. *et al.* A time-resolved, multi-symbol molecular recorder via sequential genome editing. *Nature* **608**, 98–107 (2022).
19. Michnick, S. W., Ear, P. H., Manderson, E. N., Remy, I. & Stefan, E. Universal strategies in research and drug discovery based on protein-fragment complementation assays. *Nat. Rev. Drug Discov.* **6**, 569–582 (2007).
20. Ghosh, I., Hamilton, A. D. & Regan, L. Antiparallel Leucine Zipper-Directed Protein Reassembly: Application to the Green Fluorescent Protein. *J. Am. Chem. Soc.* **122**, 5658–5659 (2000).
21. Kim, S. B., Ozawa, T., Watanabe, S. & Umezawa, Y. High-throughput sensing and noninvasive imaging of protein nuclear transport by using reconstitution of split Renilla luciferase. *Proc. Natl. Acad. Sci. U. S. A.* **101**, 11542–11547 (2004).
22. Wehr, M. C. *et al.* Monitoring regulated protein-protein interactions using split TEV. *Nat. Methods* **3**, 985–993 (2006).
23. Liu, B. *et al.* A split prime editor with untethered reverse transcriptase and circular RNA template. *Nat. Biotechnol.* (2022) doi:10.1038/s41587-022-01255-9.
24. Nelson, J. W. *et al.* Engineered pegRNAs improve prime editing efficiency. *Nat. Biotechnol.* (2021) doi:10.1038/s41587-021-01039-7.
25. Chen, P. J. *et al.* Enhanced prime editing systems by manipulating cellular determinants of editing outcomes. *Cell* **184**, 5635–5652.e29 (2021).
26. Herschlag, D. & Cech, T. R. DNA cleavage catalysed by the ribozyme from Tetrahymena. *Nature* **344**, 405–409 (1990).
27. Gambill, L., Staubus, A., Ameruoso, A. & Chappell, J. A split ribozyme that links detection of a native RNA to orthogonal protein outputs. *bioRxiv* 2022.01.12.476080 (2022) doi:10.1101/2022.01.12.476080.
28. Johansson, H. E., Liljas, L. & Uhlenbeck, O. C. RNA Recognition by the MS2 Phage Coat Protein. *Semin.*

Virol. **8**, 176–185 (1997).

29. Salstrom, J. S. & Szybalski, W. Coliphage λnutL−: A unique class of mutants defective in the site of gene N product utilization for antitermination of leftward transcription. *J. Mol. Biol.* **124**, 195–221 (1978).
30. Legault, P., Li, J., Mogridge, J., Kay, L. E. & Greenblatt, J. NMR structure of the bacteriophage lambda N peptide/boxB RNA complex: recognition of a GNRA fold by an arginine-rich motif. *Cell* **93**, 289–299 (1998).
31. Katrekar, D. *et al.* Comprehensive interrogation of the ADAR2 deaminase domain for engineering enhanced RNA editing activity and specificity. *Elife* **11**, (2022).
32. Colby, D. W. *et al.* Development of a human light chain variable domain (V(L)) intracellular antibody specific for the amino terminus of huntingtin via yeast surface display. *J. Mol. Biol.* **342**, 901–912 (2004).
33. Wörn, A. & Plückthun, A. Stability engineering of antibody single-chain Fv fragments. *J. Mol. Biol.* **305**, 989–1010 (2001).
34. Lecerf, J. M. *et al.* Human single-chain Fv intrabodies counteract in situ huntingtin aggregation in cellular models of Huntington's disease. *Proc. Natl. Acad. Sci. U. S. A.* **98**, 4764–4769 (2001).
35. Tanenbaum, M. E., Gilbert, L. A., Qi, L. S., Weissman, J. S. & Vale, R. D. A protein-tagging system for signal amplification in gene expression and fluorescence imaging. *Cell* **159**, 635–646 (2014).
36. Götzke, H. *et al.* The ALFA-tag is a highly versatile tool for nanobody-based bioscience applications. *Nat. Commun.* **10**, 4403 (2019).
37. Cabantous, S., Terwilliger, T. C. & Waldo, G. S. Protein tagging and detection with engineered self-assembling fragments of green fluorescent protein. *Nat. Biotechnol.* **23**, 102–107 (2005).
38. Banaszynski, L. A., Liu, C. W. & Wandless, T. J. Characterization of the FKBP.rapamycin.FRB ternary complex. *J. Am. Chem. Soc.* **127**, 4715–4721 (2005).
39. Bierer, B. E. *et al.* Two distinct signal transmission pathways in T lymphocytes are inhibited by complexes formed between an immunophilin and either FK506 or rapamycin. *Proc. Natl. Acad. Sci. U. S. A.* **87**, 9231–9235 (1990).
40. Brown, E. J. *et al.* A mammalian protein targeted by G1-arresting rapamycin-receptor complex. *Nature* **369**, 756–758 (1994).

41. Liang, F.-S., Ho, W. Q. & Crabtree, G. R. Engineering the ABA plant stress pathway for regulation of induced proximity. *Sci. Signal.* **4**, rs2 (2011).

42. Komor, A. C., Kim, Y. B., Packer, M. S., Zuris, J. A. & Liu, D. R. Programmable editing of a target base in genomic DNA without double-stranded DNA cleavage. *Nature* **533**, 420–424 (2016).

43. Koblan, L. W. *et al.* Improving cytidine and adenine base editors by expression optimization and ancestral reconstruction. *Nat. Biotechnol.* **36**, 843–846 (2018).

44. Richter, M. F. *et al.* Phage-assisted evolution of an adenine base editor with improved Cas domain compatibility and activity. *Nat. Biotechnol.* **38**, 883–891 (2020).

45. Qian, Y. *et al.* Programmable RNA sensing for cell monitoring and manipulation. *Nature* **610**, 713–721 (2022).

46. Kaseniit, K. E. *et al.* Modular, programmable RNA sensing using ADAR editing in living cells. *Nat. Biotechnol.* **41**, 482–487 (2023).

47. Jiang, K. *et al.* Programmable eukaryotic protein synthesis with RNA sensors by harnessing ADAR. *Nat. Biotechnol.* **41**, 698–707 (2023).

48. Chao, J. A., Patskovsky, Y., Almo, S. C. & Singer, R. H. Structural basis for the coevolution of a viral RNA-protein complex. *Nat. Struct. Mol. Biol.* **15**, 103–105 (2008).

49. Olsthoorn, R. C., Garde, G., Dayhuff, T., Atkins, J. F. & Van Duin, J. Nucleotide sequence of a single-stranded RNA phage from Pseudomonas aeruginosa: kinship to coliphages and conservation of regulatory RNA structures. *Virology* **206**, 611–625 (1995).

50. Wu, B., Chen, J. & Singer, R. H. Background free imaging of single mRNAs in live cells using split fluorescent proteins. *Sci. Rep.* **4**, 3615 (2014).

51. Slusarczyk, A. L., Lin, A. & Weiss, R. Foundations for the design and implementation of synthetic genetic circuits. *Nat. Rev. Genet.* **13**, 406–420 (2012).

52. Gordley, R. M., Bugaj, L. J. & Lim, W. A. Modular engineering of cellular signaling proteins and networks. *Curr. Opin. Struct. Biol.* **39**, 106–114 (2016).

53. Farzadfard, F. *et al.* Single-Nucleotide-Resolution Computing and Memory in Living Cells. *Mol. Cell* **75**, 769–780.e4 (2019).

54. Tang, W. & Liu, D. R. Rewritable multi-event analog recording in bacterial and mammalian cells. *Science* **360**, (2018).

55. Buenrostro, J. D. *et al.* Quantitative analysis of RNA-protein interactions on a massively parallel array reveals biophysical and evolutionary landscapes. *Nat. Biotechnol.* **32**, 562–568 (2014).

56. Baek, M., McHugh, R., Anishchenko, I., Baker, D. & DiMaio, F. Accurate prediction of nucleic acid and protein-nucleic acid complexes using RoseTTAFoldNA. *bioRxiv* 2022.09.09.507333 (2022) doi:10.1101/2022.09.09.507333.

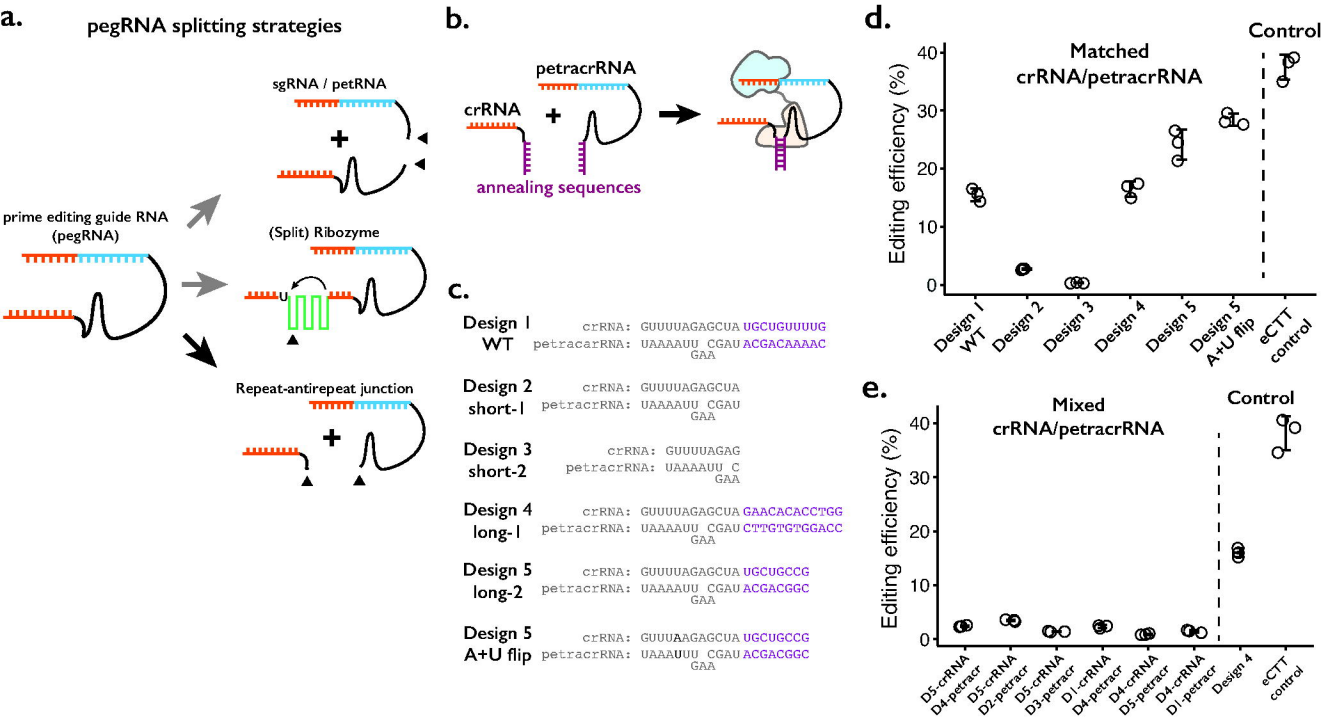
a.
pegRNA splitting strategies
sgRNA / petRNA
prime editing guide RNA
(pegRNA)
(Split) Ribozyme
U
Repeat-antirepeat junction
b.
petracrRNA
crRNA
annealing sequences
c.
Design 1
WT
crRNA: GUUUUAGAGCUA UGCUGUUUUG
petracarRNA: UAAAAUU CGAU ACGACAAAAC
GAA
Design 2
short-1
crRNA: GUUUUAGAGCUA
petracrRNA: UAAAAUU CGAU
GAA
Design 3
short-2
crRNA: GUUUUAGAG
petracrRNA: UAAAAUU C
GAA
Design 4
long-1
crRNA: GUUUUAGAGCUA GAACACACCTGG
petracrRNA: UAAAAUU CGAU CTTGTGTGGACC
GAA
Design 5
long-2
crRNA: GUUUUAGAGCUA UGCUGCCG
petracrRNA: UAAAAUU CGAU ACGACGGC
GAA
Design 5
A+U flip
crRNA: GUUUAAGAGCUA UGCUGCCG
petracrRNA: UAAAUUU CGAU ACGACGGC
GAA
d.
Matched
crRNA/petracrRNA
Control
Editing efficiency (%)
0
10
20
30
40
Design 1 WT
Design 2
Design 3
Design 4
Design 5
Design 5 A+U flip
eCTT control
e.
Mixed
crRNA/petracrRNA
Control
Editing efficiency (%)
0
10
20
30
40
D5-crRNA D4-petracr
D5-crRNA D2-petracr
D5-crRNA D3-petracr
D1-crRNA D4-petracr
D4-crRNA D5-petracr
D4-crRNA D1-petracr
Design 4
eCTT control

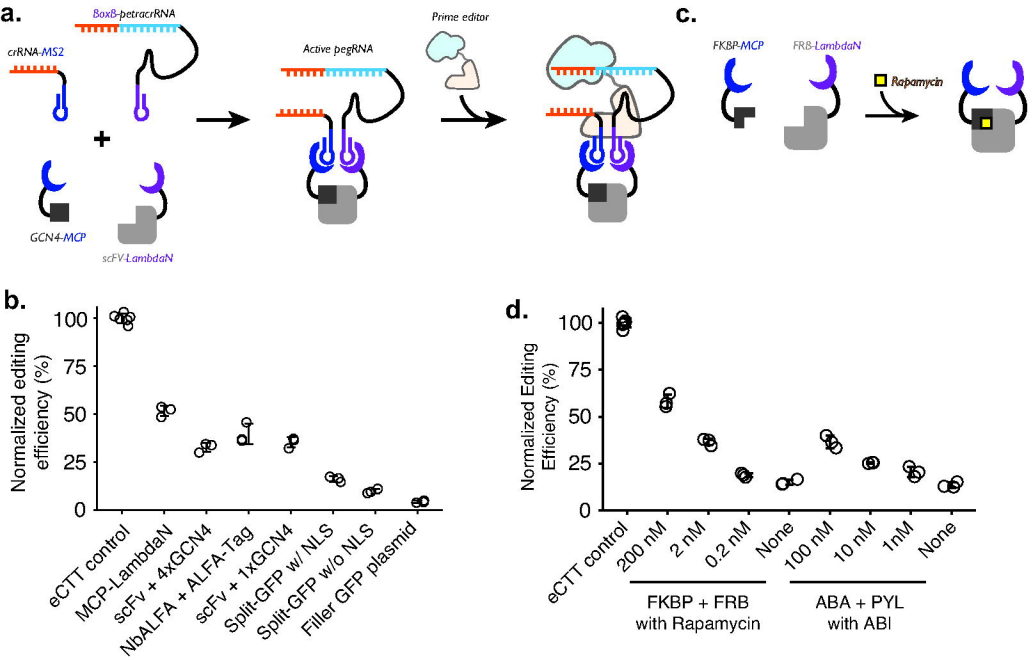
a.
8xxB-petracrRNA
crRNA-MS2
GCN4-MCP
scFV-LambdaN
Active pegRNA
Prime editor
c.
FKBP-MCP
FRB-LambdaN
Rapamycin
b.
Normalized editing efficiency (%)
100
75
50
25
0
eCTT control
MCP-LambdaN
scFv + 4xGCN4
NbALFA + ALFA-Tag
scFv + 1xGCN4
Split-GFP w/ NLS
Split-GFP w/o NLS
Filler GFP plasmid
d.
Normalized Editing Efficiency (%)
100
75
50
25
0
eCTT control
200 nM
2 nM
0.2 nM
None
100 nM
10 nM
1nM
None
FKBP + FRB with Rapamycin
ABA + PYL with ABI

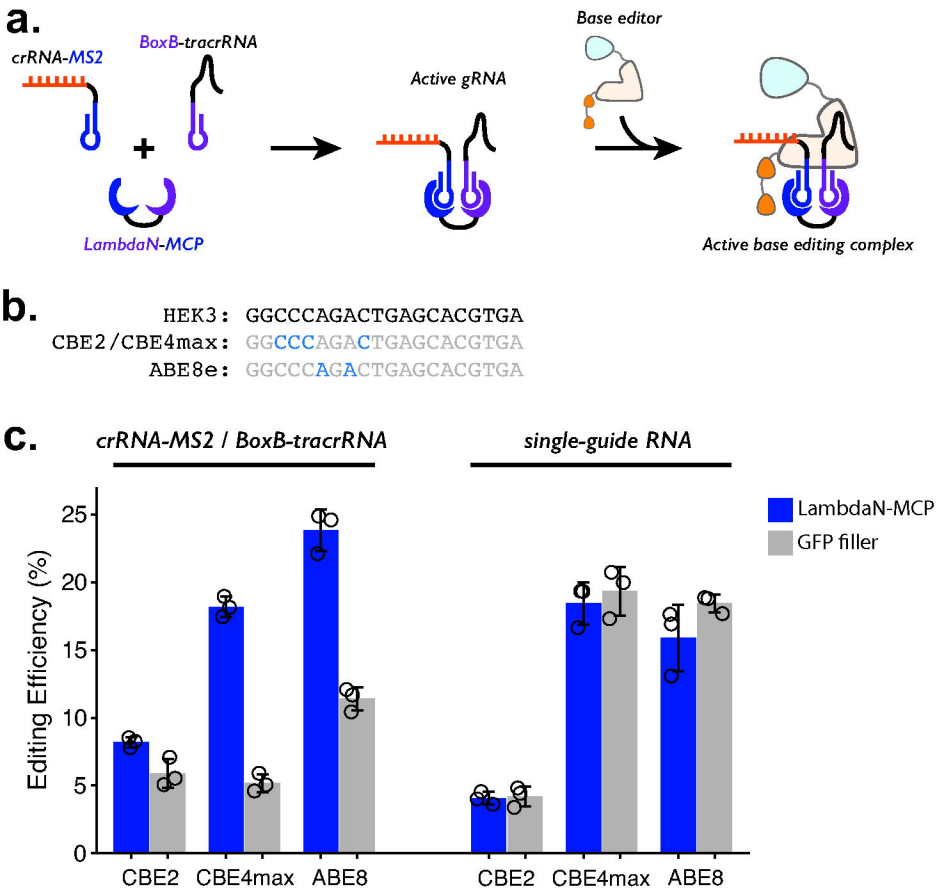
a.
crRNA-MS2
BoxB-tracrRNA
LambdaN-MCP
Active gRNA
Base editor
Active base editing complex
b.
HEK3: GGCCCAGACTGAGCACGTGA
CBE2/CBE4max: GGCCCAGACTGAGCACGTGA
ABE8e: GGCCCAGACTGAGCACGTGA
c.
crRNA-MS2 / BoxB-tracrRNA
single-guide RNA
LambdaN-MCP
GFP filler
Editing Efficiency (%)
0
5
10
15
20
25
CBE2
CBE4max
ABE8
CBE2
CBE4max
ABE8

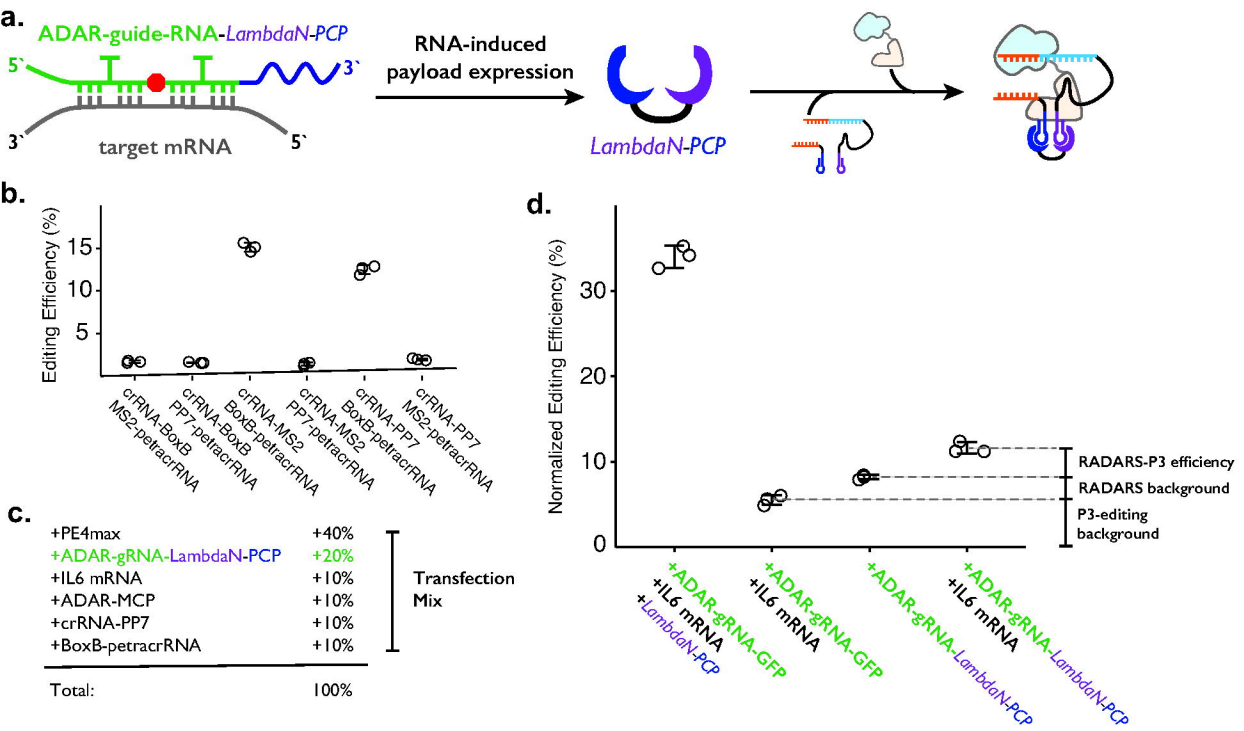
a.
ADAR-guide-RNA-LambdaN-PCP
5`
3`
3`
5`
target mRNA
RNA-induced
payload expression
LambdaN-PCP
b.
Editing Efficiency (%)
15
10
5
crRNA-BoxB
MS2-petracrRNA
crRNA-BoxB
PP7-petracrRNA
crRNA-BoxB
BoxB-petracrRNA
crRNA-MS2
PP7-petracrRNA
crRNA-MS2
BoxB-petracrRNA
crRNA-PP7
BoxB-petracrRNA
crRNA-PP7
MS2-petracrRNA
c.
+PE4max +40%
+ADAR-gRNA-LambdaN-PCP +20%
+IL6 mRNA +10%
+ADAR-MCP +10%
+crRNA-PP7 +10%
+BoxB-petracrRNA +10%
Total: 100%
Transfection
Mix
d.
Normalized Editing Efficiency (%)
30
20
10
0
RADARS-P3 efficiency
RADARS background
P3-editing
background
+IL6 mRNA
+LambdaN-PCP
+ADAR-gRNA-GFP
+IL6 mRNA
+ADAR-gRNA-GFP
+ADAR-gRNA-LambdaN-PCP
+IL6 mRNA
+ADAR-gRNA-LambdaN-PCP

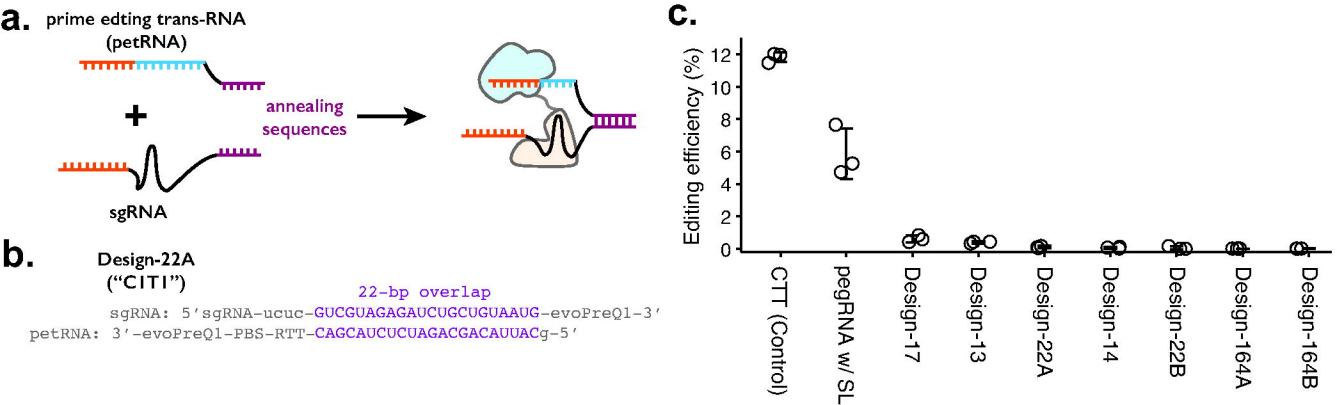
a.
prime edting trans-RNA
(petRNA)
+
sgRNA
annealing
sequences
b.
Design-22A
("CITI")
22-bp overlap
sgRNA: 5'sgRNA-ucuc-GUCGUAGAGAUCUGCUGUAAUG-evoPreQ1-3'
petRNA: 3'-evoPreQ1-PBS-RTT-CAGCAUCUCUAGACGACAUUACg-5'
c.
Editing efficiency (%)
0
2
4
6
8
10
12
CTT (Control)
pegRNA w/ SL
Design-17
Design-13
Design-22A
Design-14
Design-22B
Design-164A
Design-164B

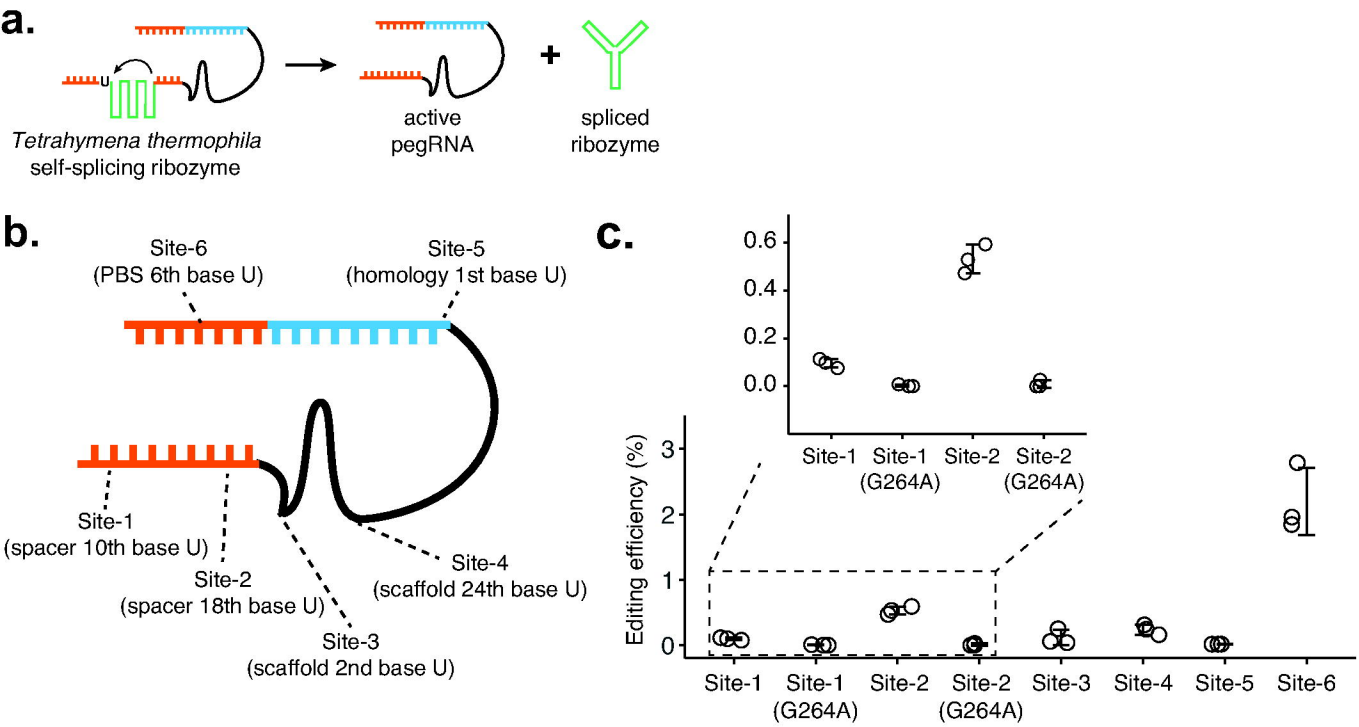
a.
U
Tetrahymena thermophila
self-splicing ribozyme
active
pegRNA
+
spliced
ribozyme
b.
Site-6
(PBS 6th base U)
Site-5
(homology 1st base U)
Site-1
(spacer 10th base U)
Site-2
(spacer 18th base U)
Site-3
(scaffold 2nd base U)
Site-4
(scaffold 24th base U)
c.
Editing efficiency (%)
0
1
2
3
0.0
0.2
0.4
0.6
Site-1
Site-1
(G264A)
Site-2
Site-2
(G264A)
Site-3
Site-4
Site-5
Site-6

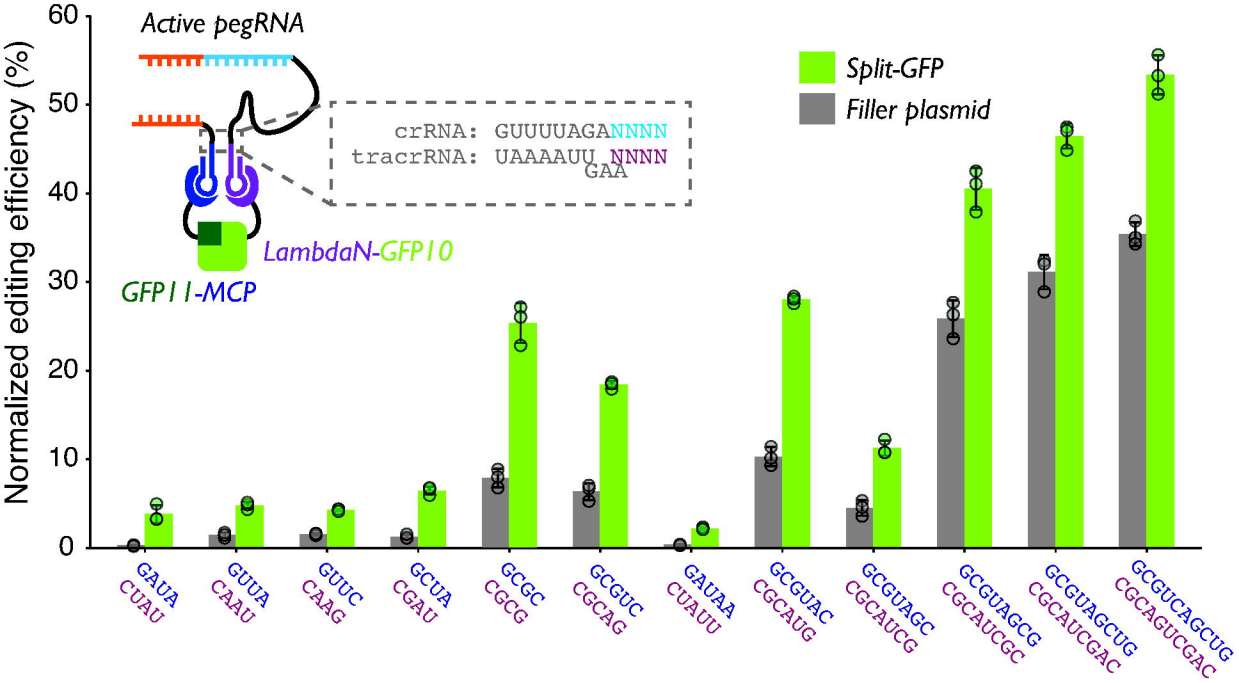
Active pegRNA
crRNA: GUUUUAGANNNN
tracrRNA: UAAAAUU NNNN
GAA
LambdaN-GFP10
GFP11-MCP
Split-GFP
Filler plasmid
Normalized editing efficiency (%)
0
10
20
30
40
50
60
GAUA CUAU
GUUA CAAU
GUUC CAAG
GCUA CGAU
GCGC CGCG
GCGUC CGCAG
GAUAA CUAUU
GCGUAC CGCAUG
GCGUAGC CGCAUCG
GCGUAGCG CGCAUCGC
GCGUAGCUG CGCAUCGAC
GCGUCAGCUG CGCAGUCGAC